4 Oxide Heterostructure Project – Observation and control of novel quantum phenomena in superstructures of strongly correlated oxides –

Project Leader: Hiroshi KUMIGASHIRA

4-1 Introduction

The goal of this project is to design novel physical properties appearing at the heterointerface of strongly correlated oxides. The physical properties arise from strong mutual coupling among the spin, charge, and orbital degrees of freedom in the interface region between two different oxides [1]. In order to control such properties, it is necessary to clarify the interfacial electronic, magnetic, and orbital structures. We are therefore using synchrotron radiation spectroscopic techniques having elemental selectivity to probe these structures in the nm-scale at the oxide heterointerface. For example, the electronic structure at the interface is determined by photoemission spectroscopy (PES) and X-ray absorption spectroscopy (XAS), the magnetic structure by magnetic circular dichroism of XAS, and the orbital structure by linear dichroism of XAS. We aim to design and create novel quantum materials by optimally combining sophisticated oxide growth techniques using laser molecular beam epitaxy (MBE) and advanced analysis techniques using quantum beams.

4-2 *In-situ* photoemission spectroscopy station for surfaces and interfaces of oxide superstructures

We have constructed and developed an "*in-situ* photoelectron spectrometer – laser molecular beam epitaxy" system where a high-resolution angle-resolved photoemission apparatus (VG-Scienta SES2002 hemispherical electron analyzer) is connected to laser-MBE equipment in ultrahigh vacuum (UHV) [2]. The system is compactly designed and can therefore be installed at several different beamlines of the Photon Factory as an endstation. A schematic view of the system is illustrated in Fig. 1.

This system consists of four interconnected chambers: sample entry, sample preparation, laser MBE, and photoemission chamber. The PES chamber is connected to a beamline. The four chambers are connected to each other in UHV and each chamber can be isolated by gate valves. A typical sequence of sample growth and measurement is as follows. First, a substrate mounted on a sample holder is loaded into the sample entry chamber and transferred to the laser MBE chamber through the sample preparation chamber. Oxide heterostructures are grown on the substrate by pulsed laser deposition while monitoring the intensity oscillation of reflection high-energy electron diffraction (RHEED). The fabricated oxide heterostructures are then transferred back to the sample preparation chamber where their surface structure and surface cleanness can be characterized by low-energy electron diffraction (LEED) and Auger electron spectroscopy (AES). After surface characterization, the sample is moved with a transfer rod into the photoemission measurement stage. The sample transfer is carefully operated under UHV of 10^{-10} Torr in order to avoid contamination of the surface of the sample during the transfer. Such *in-situ* photoemission analysis is crucial for investigating the physical properties of oxide thin films and heterostructures, and few research groups have the capability to perform such experiments in a synchrotron facility [3]. Thus, our system is important for research in the field of strongly-correlated oxide heterostructures.

4-3 Construction of new beamlines for surface and interface studies of oxide superstructures

Previously, we had mainly used the *in-situ* PES – laser MBE system either at BL-28 for angle-resolved photoemission spectroscopy in the vacuum ultraviolet (VUV) region or at BL-2C for photoemission spectroscopy and X-ray absorption spectroscopy in the soft X-ray (SX) region. In order to enhance studies of

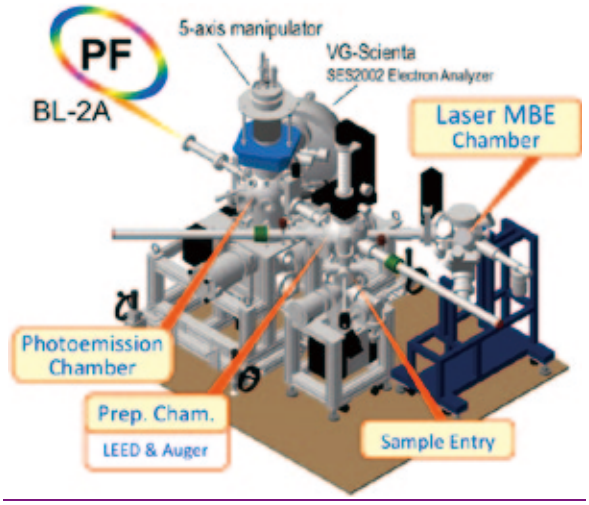

Fig. 1: Schematic view of the developed "*in-situ* PES – laser MBE" system. This system will be installed at a new undulator beamline, BL-2A, which is designed for surface and interface studies of oxide heterostructures.

the surfaces and interfaces of oxide heterostructures, we scrapped the old BL-2C beamline and started constructing the new BL-2A (Fig. 2). This new beamline has two types of undulator in tandem alignment; one is designed for the VUV region (30–300 eV), and the other for the SX region (250–2000 eV). Consequently, relatively wide energy-range light while maintaining high brilliance and high energy resolution will be available in this beamline by the combination of the two undulators and a variable-included-angle varied-line-spacing plane-grating (VLSPG) monochromator. The instrument will be installed at the new undulator beamline BL-2A as an endstation (at FA1 port in Fig. 2).

4-4 Science topic: Gradual localization of Ni 3*d* states in $LaNiO_3$ ultrathin films induced by dimensional crossover

Immediately after the similarity between the electronic structures of the $LaNiO_3/LaAlO_3$ superlattice and those of high-*Tc* cuprates [4-6] was predicted, a number of experiments explored possible high-*Tc* superconductivity in heterostructures based on $LaNiO_3$ (LNO) [7-11]. The theory predicted the emergence of two-dimensional electron liquid states in the LNO layer as a result of the quantum confinement of Ni 3*d* electrons [5,6]. The resultant dx^2-y^2 orbital ordering produces a single Fermi surface resembling that in the cuprates. However, almost all experiments reported that the heterostructures or ultrathin films underwent the transition from metal to insulator at a critical LNO-layer thickness of 3–5 monolayers (ML) [7-11], strongly suggesting the intrinsic insulating ground states of the LNO layer at a thin limit.

Despite intensive theoretical and experimental studies [9-15], the origin of the thickness-dependent metal-insulator transition (MIT) in the LNO layer remains unclear, and the fundamental origin of the insulating ground states of LNO ultrathin films has attracted much discussion. One of the scenarios proposed for describing the physics of the insulating ground states is "dimensional-crossover-driven MIT" [16]. According to this scenario (see Fig. 3), a decrease in the layer thickness of LNO causes a reduction in the effective bandwidth *W* owing to the prevention of charge transfer at the interface and the surface. The resultant reduction in *W* from a three-dimensional thick film (layer) to a two-dimensional ultrathin film (layer) may drive MIT in an LNO film (a superlattice based on LNO) at a thin limit.

On the other hand, it is well known that rare-earth nickel perovskites ($RNiO_3$, where *R* = rare earth) exhibit insulating ground states as a result of temperature-driven MIT for most rare-earth ions except La [17]. The transition temperature increases with decreasing size of the *R* ion, suggesting that the gap opening would be due to a smaller Ni-O-Ni superexchange angle, leading to a reduction in *W*. The similar "bandwidth reduction" scenario is applicable to the insulating ground states in LNO ultrathin films [17]: the possible octahedral tilts and rotations due to the structural influence from substrates make the Ni-O-Ni superexchange angle smaller at an interface region, and the resultant reduction in *W* may cause the insulating ground states in LNO films at a thin limit. However, recent studies have revealed that charge disproportionation ($2Ni^{3+} \rightarrow Ni^{3+\delta} + Ni^{3-\delta}$) is also responsible for the insulating ground states in all the members of $RNiO_3$ [18,19]. The first-order temperature-driven MIT accompanied by a structural change from orthorhombic to monoclinic phase is characteristic of the MIT in $RNiO_3$.

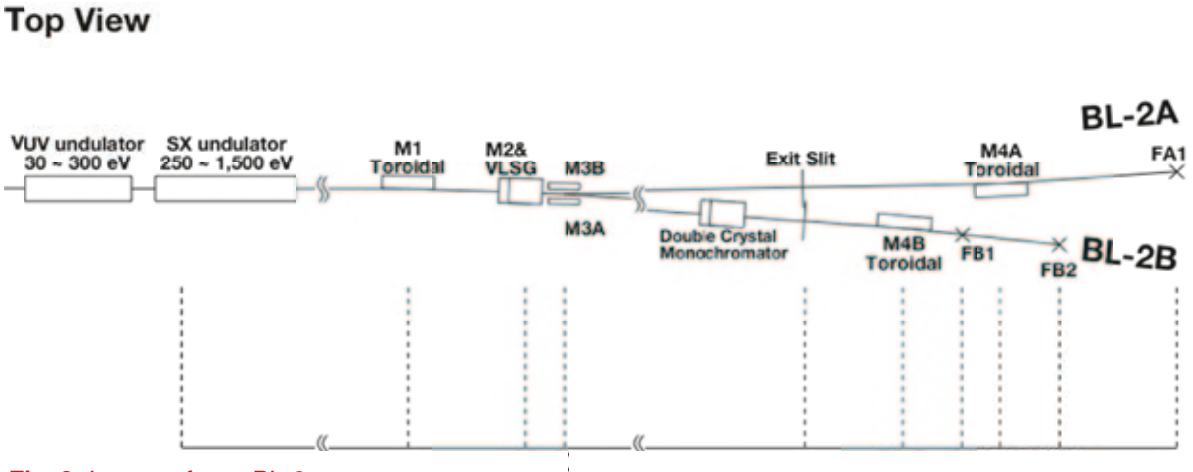

Fig. 2: Layout of new BL-2.

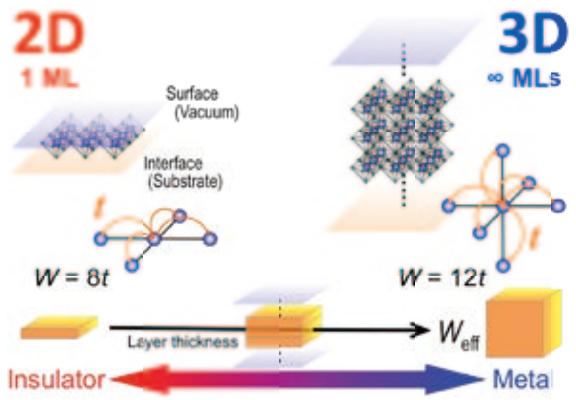

Fig. 3: Schematic of the concept for dimensional-crossover-driven MIT occurring in an artificial structure.

In contrast, the thickness-dependent MIT in LNO is marked by gradually localized behavior with a reduction in the LNO layer thickness. The LNO layer transforms from metallic to insulating states through intermediate localized states (bad metal or variable-range-hopping (VRH) regimes) with decreasing LNO layers [7-11]. The gradually localized behavior in the transport properties of LNO contrasts sharply with the temperature-driven MIT in other RNiO$_3$ [17], suggesting the absence or strong suppression of the charge-disproportionate states in insulating states of LNO layers, plausibly as a result of epitaxial strain.

To understand the origin of the thickness-dependent MIT in LNO as well as the insulating ground states at a thin limit, it is crucial to obtain information on how the electronic structures change as a function of layer thickness, especially information on the possible evolution of charge disproportionation across the MIT, which is characteristic of the insulating states of bulk RNiO$_3$. Thus, we address these questions through *in-situ* PES and XAS measurements on LNO ultrathin films grown on LaAlO$_3$ (LAO) substrates with varying film thickness [20].

Digitally controlled LNO ultrathin films were grown on the (001) surface (in terms of the pseudocubic description) of an LAO substrate in a laser MBE chamber (see Fig. 1). During deposition, the substrate temperature was maintained at 450ºC under an oxygen pressure of 10^{-3} Torr. The film thickness was precisely controlled on the atomic scale by monitoring the intensity oscillation of RHEED as shown in Fig. 4(a). The LNO thin films were subsequently annealed at 400ºC for 45 min in oxygen at atmospheric pressure to remove oxygen vacancies. The absence of oxygen vacancies was also confirmed by *in-situ* O 1*s* XAS measurements [20,21].

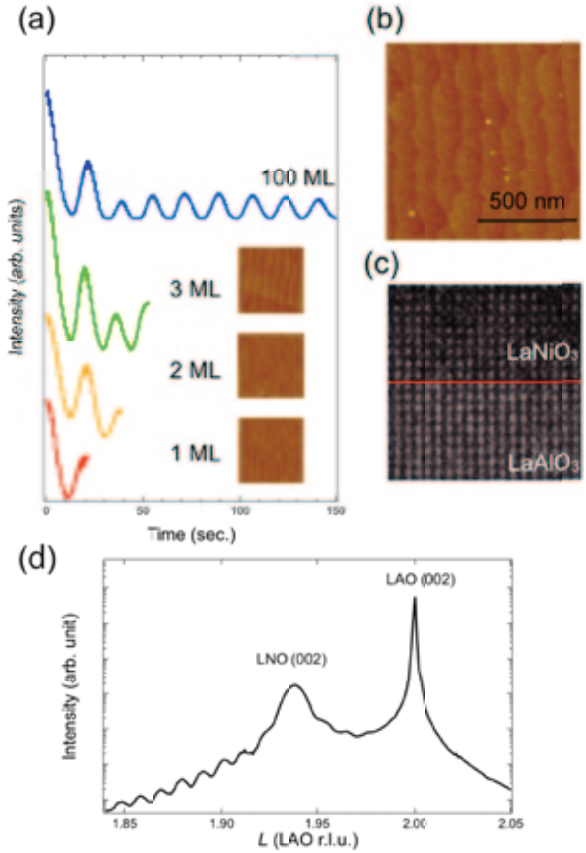

Fig. 4: Characterizations of LaNiO$_3$ films grown on LaAlO$_3$ substrates: (a) Typical RHEED intensity oscillations and corresponding AFM images (scan area 1 x 1 μm^2). (b) A typical AFM image of LNO films (100 ML). (c) Cross-sectional TEM image of the interface between LNO and LAO. The line indicates the interface between the two. (d) Synchrotron based XRD pattern along the (00*L*) scan around the (002) reflections of an LNO film (100 ML) and an LAO substrate.

The PES measurements were performed *in situ* with a total energy resolution of 120 meV at room temperature. The XAS spectra were also measured *in situ* in the total electron-yield mode. The surface morphology of the measured films was analyzed by *ex situ* atomic force microscopy (AFM) in air [Fig. 4(b)]. The crystal structure was characterized by cross-sectional transmission electron microscopy (TEM) [Fig. 4(c)] and synchrotron based X-ray diffraction (XRD) [Fig. 4(d)] measurements performed at BL4C of the Photon Factory. These characterization results guarantee the formation of an atomically flat surface and chemically abrupt interface of LNO/LAO heterostructures, as well as the coherent growth of LNO onto LAO substrates while maintaining high crystal quality.

Figure 5(a) shows the valence-band spectra of LNO ultrathin films grown on LAO substrates by digitally

controlling the LNO layer thickness. Since the LAO substrate has a wide band gap of 5.6 eV, the electronic structure near the Fermi level (E_F) of LNO films is not influenced by a signal from the substrate even for ultrathin films. In films thicker than 20 ML, the line shapes of these spectra are almost identical to each other. The valence-band spectra consist of two structures: two sharp structures derived from Ni e_g and t_{2g} states located at E_F and 0.8 eV, respectively, and broad O-2*p* derived structures with a binding energy of 2–7 eV [21]. It should be noted that such a sharp two-peak structure of Ni 3*d* states near E_F has only been observed in a previous *in-situ* PES measurement on an LNO thick film having an atomically flat surface [21] and a bulk sensitive hard X-ray PES measurement on an LNO film grown on LAO substrates [22]. This attests to the high quality of the surfaces of the LNO ultrathin films measured in the present study.

When the film thickness is decreased to below 10 ML, the valence-band spectra show remarkable and systematic changes mainly at Ni 3*d* states near E_F. To investigate the changes in Ni 3*d* states in more detail, we present the near-E_F spectra according to an enlarged binding energy scale in Fig. 5(b). For film thicknesses of 3–10 ML, the intensity of the Ni-3*d*-derived peak at E_F gradually decreases, and simultaneously the t_{2g} peak broadens. The leading edge of the Ni 3*d* states appears to shift from above E_F to below E_F at 3–6 ML, suggesting the evolution of a pseudogap at E_F. As the film thickness is decreased further, the density of states (DOS) at E_F becomes negligible, and finally a clear energy gap opens at 1–2 ML. An extrapolation of the linear portion of the leading edge to the energy axis yields a valence-band maxima of 200 meV for a 1-ML film and almost 0 meV for a 2-ML film. The negligibly small residual DOS at E_F for the 2-ML film may be due to the finite energy resolution of our experimental system (120 meV). These results indicate the occurrence of MIT at a critical thickness of 2–3 ML.

It should be noted that the observed spectral behaviors are in line with the results of transport measurements [7-11,20]. Therefore, the present PES results demonstrate that LNO ultrathin films transform from metal to insulator through an intermediate state. The existence of the intermediate state, which is characterized by the gradual localization of conduction carriers from weak localization (Anderson localization behavior) to strong localization (VRH behavior) in films with thicknesses of 4–10 ML, is considered to be the key factor for understanding the origin of the peculiar insulating state in LNO ultrathin films [9,11]. Since these intermediate states seem to have a close relationship with the formation of a pseudogap

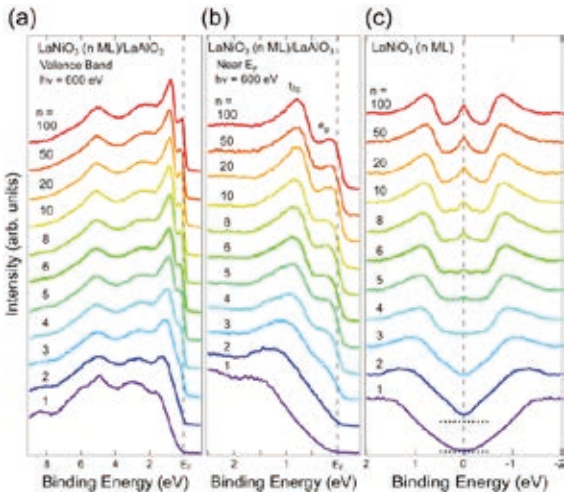

Fig. 5: (a) *In-situ* valence-band spectra of LNO ultrathin films grown on LAO substrates by digitally controlling the film thickness. (b) PES spectra near E_F. (c) Symmetrized spectra near E_F.

observed in the present PES measurements, a more detailed analysis of the pseudogap is required to understand the origin of the MIT.

To clarify the formation of the energy gap and pseudogap, we symmetrized the near-E_F spectra with respect to E_F to remove the effects of the Fermi-Dirac function on the spectra [16]. The resultant symmetrized spectra are shown in Fig. 5(c). As expected from the raw data in Fig. 5(b), the change in the spectra is mainly caused by the suppression of the quasiparticle peak at E_F and subsequent formation of a pseudogap and a gap. In films thicker than 20 ML, a sharp quasiparticle peak is located just at E_F and remains almost unchanged irrespective of film thickness. In contrast, below 10 ML the intensity of quasiparticle peaks monotonically decreases with film thickness. As a result of the suppression of spectral intensity at E_F, a pseudogap structure is apparently formed at E_F below 4 ML. Finally, the DOS at E_F disappears at a film thickness of 1–2 ML, leading to the formation of an energy gap. These results clearly illustrate that the evolution of the pseudogap and the resultant formation of the energy gap at E_F are responsible for the MIT in LNO ultrathin films through the intermediate localized states.

Next, we address a fundamental question as to whether the observed thickness-dependent MIT is accompanied by charge disproportionation as observed in other RNiO$_3$ family members. Charge disproportionation concomitant with resultant structural change has been commonly observed for all the members of RNiO$_3$, except LNO, across the temperature-driven MIT [18,19]. Since the charge disproportionation in bulk RNiO$_3$ modulates the local

electronic structure around Ni^{3+} ions, the line shape of elementally selective Ni *L*-edge XAS spectra is very sensitive to the occurrence of the charge disproportionation: the characteristic shoulder structure emerges across the transition from the orthorhombic metallic state to the monoclinic insulating state. Thus, Ni *L*-edge XAS has been used as an indicator of the charge disproportionate ion state in $RNiO_3$ [6,23].

Figure 6 shows *in-situ* Ni L_2-edge XAS spectra of LNO ultrathin films with a film thickness around the critical film thickness of the MIT. We focus on the Ni L_2 edge to verify the occurrence of charge disproportionation, since the Ni L_3-edge structure overlaps the La M_4 edge because of the close proximity of the two energy levels [23]. The XAS spectra of bulk $NdNiO_3$ for both metallic and insulating states are also shown in Ref. 23. For bulk $NdNiO_3$, a clear additional shoulder structure at ~869 eV, indicative of charge disproportionation, appears across the transition from metallic to insulating state, as observed in the Ni L_2-edge spectra of other bulk $RNiO_3$ members.

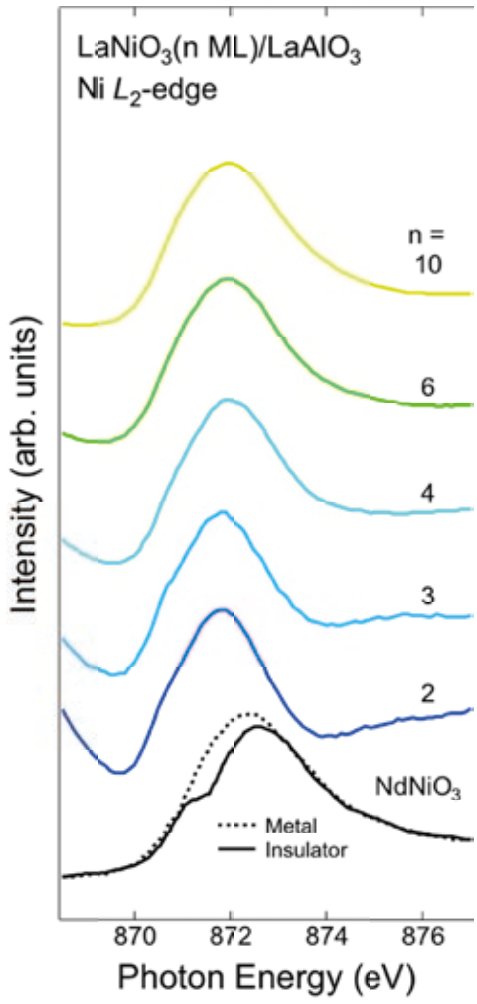

Fig. 6: *In-situ* XAS spectra at the Ni L_2 edge of LNO ultrathin films on LAO substrates, together with those of a $NdNiO_3$ bulk sample in the metallic (dotted line) and insulating (solid line) states (Ref. 23).

The spectral shape of LNO ultrathin films in the that of metallic $NdNiO_3$. In contrast, the spectra of insulating LNO ultrathin films below 3 ML exhibit significant differences from insulating $NdNiO_3$: the characteristic low-energy shoulder structure observed in insulating $NdNiO_3$ is almost absent in the insulating phase of LNO ultrathin films. Although a negligibly weak low-energy shoulder structure reminiscent of charge disproportionation seems to exist, this structure may originate from the structural modulation at the interface and/or surface as a result of the reduction in Ni-O covalency at the surface and/or the interface between the film and substrate [9]. Thus, from the XAS measurements on the Ni *L* edge, charge disproportionation as observed in bulk $RNiO_3$ is strongly suppressed in the insulating states of LNO ultrathin films. The suppression of charge disproportionation is plausibly a result of epitaxial strain, since similar suppression of charge disproportionation in epitaxial films has been reported for $NdNiO_3$: in an epitaxial film coherently grown on a substrate, the in-plane lattice constant is locked to that of the substrate, and consequently such an epitaxial strain effect should hinder a first-order MIT accompanied by a structural change [23]. Although we cannot entirely eliminate the possibility of other spin- and/or charge-ordered states for insulating ground states of LNO ultrathin films via the present experiment, it is reasonable to conclude that the intrinsic insulating ground states in LNO ultrathin films can be described as novel insulators where the charge disproportionation has a minor contribution.

References

[1] H. Y. Hwang et al., Nat. Mater. **11**, 103 (2012).
[2] K. Horiba et al., Rev. Sci. Instrum. **74**, 3406 (2003).
[3] R. Ramesh et al., Nat. Mater. **6**, 21 (2007).
[4] J. Chaloupka et al., Phys. Rev. Lett. **100**, 016404 (2008).
[5] P. Hansmann et al., Phys. Rev. Lett. **103**, 016401 (2009).
[6] P. Hansmann et al., Phys. Rev. B **82**, 235123 (2010).
[7] J. Son et al., Appl. Phys. Lett. **96**, 062114 (2010).
[8] J. Son et al., Appl. Phys. Lett. **97**, 202109 (2010).
[9] J. Liu et al., Phys. Rev. B **83**, 161102 (2011).
[10] R. Scherwitzl et al., Appl. Phys. Lett. **95**, 222114 (2009).
[11] R. Scherwitzl et al., Phys. Rev. Lett. **106**, 246403 (2011).
[12] A. V. Boris et al., Science **332**, 937 (2011).

[13] E. Benckiser et al., Nat. Mater. **10**, 189 (2011).
[14] A. M. Kaiser et al., Phys. Rev. Lett. **107**, 116402 (2011).
[15] A. Blanca-Romero et al., Phys. Rev. B **84**, 195450 (2011).
[16] K. Yoshimatsu et al., Phys. Rev. Lett. **104**, 147601 (2010).
[17] J. B. Torrance et al., Phys. Rev. B **45**, 8209 (1992).
[18] J. A. Alonso et al., Phys. Rev. Lett. **82**, 3871 (1999).
[19] J. A. Alonso et al., Phys. Rev. B **61**, 1756 (2000).
[20] E. Sakai et al., Phys. Rev. B **87**, 075132 (2013).
[21] K. Horiba et al., Phys. Rev. B **76**, 155104 (2007).
[22] A. X. Gray et al., Phys. Rev. B **84**, 075104 (2011).
[23] J. Liu et al., Appl. Phys. Lett. **96**, 233110 (2010).